Atmospheric Research 169 (2016) 54–64

Contents lists available at ScienceDirect

Atmospheric Research

journal homepage: www.elsevier.com/locate/atmos

A three-dimensional WRF-based precipitation equation and its application in the analysis of roles of surface evaporation in a torrential rainfall event

Yongjie Huang [a,b], Xiaopeng Cui [a,d,*], Xiaofan Li [c]

[a] Key Laboratory of Cloud-Precipitation Physics and Severe Storms (LACS), Institute of Atmospheric Physics, Chinese Academy of Sciences, Beijing, China
[b] University of Chinese Academy of Sciences, Beijing, China
[c] Department of Earth Sciences, Zhejiang University, Hangzhou, Zhejiang, China
[d] Collaborative Innovation Center on Forecast and Evaluation of Meteorological Disasters, Nanjing University of Information Science & Technology, Nanjing, China

ARTICLE INFO

Article history:
Received 12 June 2015
Received in revised form 2 September 2015
Accepted 27 September 2015
Available online 9 October 2015

Keywords:
WRF-based surface precipitation equation
Surface evaporation
Surface rainfall processes
Torrential rainfall

ABSTRACT

Based on the governing equations for water species in the Weather Research and Forecasting (WRF) model, a three-dimensional WRF-based surface precipitation equation was obtained and applied to investigate the surface rainfall processes of a torrential rain event. Sensitivity experiments were performed to further explore roles of surface evaporation in the heavy rainfall event. The results show that the contributions of moisture-related processes to precipitation (Q_{WV}, including water vapor local change (Q_{WVL}), surface evaporation (Q_{WVE}), moisture advection (Q_{WVA}), and so on) dominate the torrential rain event, while the contributions of cloud-related processes (Q_{CM}) also play indispensable roles whose maximum net contributions could exceed 20%. Q_{WVA} dominates the budget of water vapor, while Q_{WVL} and Q_{WVE} play smaller but by no means negligible roles in the event. Sensitivity experiments show that the changes of surface evaporation affect both moisture-related processes and cloud-related processes, and then influence the intensity and regional redistribution of precipitation. Surface evaporation favors the accumulation of convective available potential energy and enhances the instability of atmosphere, being prone to the development of convective systems. Meanwhile, it also affects the development of vertical motions and cloud systems. Thus accurate estimation of surface evaporation is necessary for accurate simulation and forecast of surface precipitation.

1. Introduction

Precipitation, especially torrential rainfall, has important impact on people's daily life, development of society and economy. Torrential rainfall, occurring in mountainous regions in particular, can cause floods, debris flows and other natural disasters, leading to tremendous losses in lives and properties of people.

Precipitation is produced from interactions among large-scale or synoptic-scale dynamic, thermodynamic and cloud microphysical processes. Precipitation-related physical processes include moisture budget and cloud hydrometeor budget. In numerical models, the moisture budget is depicted by the governing equation of water vapor and the cloud hydrometeor budget is depicted by governing equations of various liquid-phase and ice-phase hydrometeors. Gao et al. (2005) derived a diagnostic equation, called surface rainfall equation, in a two-dimensional (2D) cloud-resolving model (CRM) framework by combining the water vapor budget with the cloud hydrometeor budget. In their 2D CRM-based surface rainfall equation, surface rain rate is directly connected and determined by water vapor related processes (water vapor budget) and cloud-related processes (cloud hydrometeor budget). The moisture-related processes include local change of water vapor, water vapor convergence/divergence, and surface evaporation. The cloud-related processes include local change of cloud hydrometeors and hydrometeor convergence/divergence. They found that both moisture-related and cloud-related processes have important contributions to tropical surface rainfall. The 2D CRM-based surface rainfall equation has been widely applied to quantitatively diagnose and analyze precipitation processes, especially tropical ones (Cui, 2008, 2009; Cui and Li, 2006, 2009; Gao et al., 2009; Gao and Li, 2008a, 2010; Li, 2006; Shen et al., 2011a,2011b,2011c; Wang et al., 2007). Cui and Li (2006) investigated the role of surface evaporation in tropical surface rainfall processes using the 2D CRM-based surface rainfall equation. They found that the moisture from surface evaporation over rainfall-free regions supplies rainfall regions via moisture advection and then produces the surface rainfall. Li (2006) investigated precipitation responses to large-scale forcing in tropical deep convective regimes using the same 2D equation. He found that the moisture-related sources

* Corresponding author at: Key Laboratory of Cloud-Precipitation Physics and Severe Storms (LACS), Institute of Atmospheric Physics, Chinese Academy of Sciences, Beijing 100029, China.
E-mail address: xpcui@mail.iap.ac.cn (X. Cui).

http://dx.doi.org/10.1016/j.atmosres.2015.09.026
0169-8095/

determine the surface rain rate in the strong-forcing case, while cloud-related processes could become important in the weak-forcing case. The 2D CRM-based surface rainfall equation has also been used to study the surface rainfall processes of monsoonal convection (Wang et al., 2007), oceanic convection and its diurnal variations in tropical western Pacific (Gao et al., 2009; Gao and Li, 2010), and the effects of vertical wind shear and cloud radiation processes of a pre-summer heavy rainfall event over Southern China (Shen et al., 2011b).

The surface rainfall/precipitation equation, involving both water vapor and cloud hydrometeor budgets, is very useful and important to improve the understanding of complex precipitation processes. Based on this equation, individual precipitation processes are well understood from explicit cloud-resolving model simulations. However, most of the above studies were performed in tropical regions, and all of the studies were carried out using the above 2D CRM-based surface rainfall equation (Gao et al., 2005) in a 2D CRM framework, in which spatially uniform large-scale advection tendencies and zonal winds were imposed to force the model integration (Gao and Li, 2008a,2008b).

Two-dimensional CRMs have been used in many pioneering studies (Krueger, 1988; Xu et al., 1992; Xu and Randall, 1996). The 2D and 3D CRMs may produce similar simulations in terms of thermodynamic fields, vertical transports of mass, moisture, surface heat fluxes, and surface precipitation (Grabowski et al., 1998; Tao et al., 1987; Tompkins, 2000). Xu et al. (2002) found that there should be some differences between 2D and 3D dynamics through an intercomparison study of eight 2D and two 3D CRMs' simulations. As mentioned in Xu et al. (2002, 2005), the energy cascade is different between 2D and 3D convections, and the horizontal hydrometeor advection can impact the timing of convection. Tompkins (2000) also found that a 2D model may give reasonable results for modeling highly two-dimensionally organized convection, but it is highly preferable to use a 3D cloud model for modeling randomly distributed or clustered convection. In CRMs, the lateral periodic boundary-layer condition does not allow convection to propagate out or advect into the domain, which is not realistic, while it is not the case in the Weather Research and Forecasting (WRF) model (Skamarock et al., 2008) used in this study. Spatially varying large-scale forcing in simulations using the WRF model could also produce different dynamic and thermodynamic structures of atmosphere from the spatially uniform large-scale forcing imposed in the CRMs, affecting the cloud processes and then the surface precipitation processes. Thus, precipitation equation should be extended to 3D framework and 3D cloud-scale models (such as the WRF model) rather than CRMs should be used to study surface rainfall processes in a more realistic way. This is because 3D settings allow aperiodic boundary-layer condition, spatially varying large-scale vertical velocities and detailed hydrometeor advections.

As is well known, surface evaporation is indispensable to long-term regional or global precipitation, while roles of surface evaporation in short-term rainfall processes over land have not been thoroughly investigated, especially heavy ones. Cui and Li (2006) pointed out in their 2D CRM study that surface evaporation is very important to long-term tropical rainfall processes. Paegle et al. (1996) found that surface evaporation was more important in changing the buoyancy for short-term rainfall than in providing additional moisture to the already abundant moisture influx from the Gulf of Mexico during the 1993 United States summer floods. Cui and Li (2011) found that surface evaporation played a minor role in short-term tropical surface rainfall processes based on 2D cloud-resolving simulation data. Therefore, further discussion and research on roles of surface evaporation in short-term heavy rainfall events should be conducted.

In this study, a 3D WRF-based surface precipitation equation was obtained from the governing equations for water species in the WRF model and applied to investigate the surface rainfall processes, especially the roles of surface evaporation in a torrential rain event in Sichuan, China. The 3D WRF-based surface precipitation equation is described in Section 2. The surface rainfall processes and roles of surface evaporation in the torrential rainfall event are presented in Section 3. Summary and conclusions are given in Section 4.

2. 3D WRF-based surface precipitation equation

To examine complicated surface rainfall processes, Gao et al. (2005) derived the 2D CRM-based surface rainfall equation. In this section, a 3D WRF-based surface precipitation equation is obtained accordingly. The governing equations for water species in the WRF model (Skamarock et al., 2008) are expressed as:

$$\frac{\partial(\rho_a Q_v)}{\partial t} = \mathrm{ADV}_{Q_v} + \mathrm{DIFF}_{Q_v} + E_S + \rho_a S_{Q_v}, \tag{1}$$

$$\frac{\partial(\rho_a Q_c)}{\partial t} = \mathrm{ADV}_{Q_c} + \mathrm{DIFF}_{Q_c} + \rho_a S_{Q_c}, \tag{2}$$

$$\frac{\partial(\rho_a Q_x)}{\partial t} = \mathrm{ADV}_{Q_x} + \mathrm{DIFF}_{Q_x} + \mathrm{SEDI}_{Q_x} + \rho_a S_{Q_x}, x\in(\mathrm{r,i,s,g,h}). \tag{3}$$

The 3D advection terms are expressed as $\mathrm{ADV}_{Q_v} = -\nabla_3\cdot(\rho_a Q_v \mathbf{V})$, $\mathrm{ADV}_{Q_c} = -\nabla_3\cdot(\rho_a Q_c \mathbf{V})$, and $\mathrm{ADV}_{Q_x} = -\nabla_3\cdot(\rho_a Q_x \mathbf{V})$, and the sedimentation term is expressed as $\mathrm{SEDI}_{Q_x} = \frac{\partial(\rho_a Q_x V_{Q_x})}{\partial z}$, where Q_v, Q_c, and Q_x are the mixing ratios of water species (v: water vapor; c: cloud water; r: rain water; i: cloud ice; s: snow; g: graupel; h: hail), E_S is the surface moisture flux, ρ_a is the air density, $\mathbf{V}$ is the 3D wind vector, V_{Q_x} is the mass-weighted terminal particle fall speed, and S_{Q_v}, S_{Q_c}, and S_{Q_x} are source and sink terms.

Since all of the source/sink terms satisfy (Skamarock et al., 2008)

$$S_{Q_v} + S_{Q_c} + \sum_{x\in(\mathrm{r,i,s,g,h})} S_{Q_x} = 0, \tag{4}$$

combining Eqs. (1)–(4), we can get:

$$\begin{aligned} -\sum_{x\in(\mathrm{r,i,s,g,h})}\mathrm{SEDI}_{Q_x} &= -\frac{\partial(\rho_a Q_v)}{\partial t} + \mathrm{ADV}_{Q_v} + \mathrm{DIFF}_{Q_v} + E_S \\ &+ \sum_{x\in(\mathrm{c,r})}\left[-\frac{\partial(\rho_a Q_x)}{\partial t}\right] + \sum_{x\in(\mathrm{c,r})}\left(\mathrm{ADV}_{Q_x} + \mathrm{DIFF}_{Q_x}\right) \\ &+ \sum_{x\in(\mathrm{i,s,g,h})}\left[-\frac{\partial(\rho_a Q_x)}{\partial t}\right] + \sum_{x\in(\mathrm{i,s,g,h})}\left(\mathrm{ADV}_{Q_x} + \mathrm{DIFF}_{Q_x}\right). \end{aligned} \tag{5}$$

Integrating Eq. (5) using $\int_{z_s}^{z_t}()dz$ (where z_t and z_s are the top and surface of the model atmosphere, respectively), we get the 3D WRF-based surface precipitation equation:

$$\begin{aligned} \int_{z_s}^{z_t}\Bigg(-\sum_{x\in(\mathrm{r,i,s,g,h})}\mathrm{SEDI}_{Q_x}\Bigg)dz &= \underbrace{\int_{z_s}^{z_t}\left[-\frac{\partial(\rho_a Q_v)}{\partial t}\right]dz}_{Q_{WVL}} + \underbrace{\int_{z_s}^{z_t}\mathrm{ADV}_{Q_v}dz}_{Q_{WVA}} + \underbrace{\int_{z_s}^{z_t}\mathrm{DIFF}_{Q_v}dz}_{Q_{WVD}} + \underbrace{\int_{z_s}^{z_t}E_S dz}_{Q_{WVE}} \\ &= \underbrace{P_S}_{} \\ &+ \underbrace{\int_{z_s}^{z_t}\left[-\sum_{x\in(\mathrm{c,r})}\frac{\partial(\rho_a Q_x)}{\partial t}\right]dz}_{Q_{CLL}} + \underbrace{\int_{z_s}^{z_t}\sum_{x\in(\mathrm{c,r})}\mathrm{ADV}_{Q_x}dz}_{Q_{CLA}} + \underbrace{\int_{z_s}^{z_t}\sum_{x\in(\mathrm{c,r})}\mathrm{DIFF}_{Q_x}dz}_{Q_{CLD}} \\ &+ \underbrace{\int_{z_s}^{z_t}\left[-\sum_{x\in(\mathrm{i,s,g,h})}\frac{\partial(\rho_a Q_x)}{\partial t}\right]dz}_{Q_{CIL}} + \underbrace{\int_{z_s}^{z_t}\sum_{x\in(\mathrm{i,s,g,h})}\mathrm{ADV}_{Q_x}dz}_{Q_{CIA}} + \underbrace{\int_{z_s}^{z_t}\sum_{x\in(\mathrm{i,s,g,h})}\mathrm{DIFF}_{Q_x}dz}_{Q_{CID}}. \end{aligned} \tag{6}$$

The equation can be simply expressed as:

$$P_S = Q_{WV} + Q_{CM}, \tag{7}$$

where $P_S = \int_{z_s}^{z_t}(-\sum_{x\in(\mathrm{r,i,s,g,h})}\mathrm{SEDI}_{Q_x})dz$ is the surface rain rate.

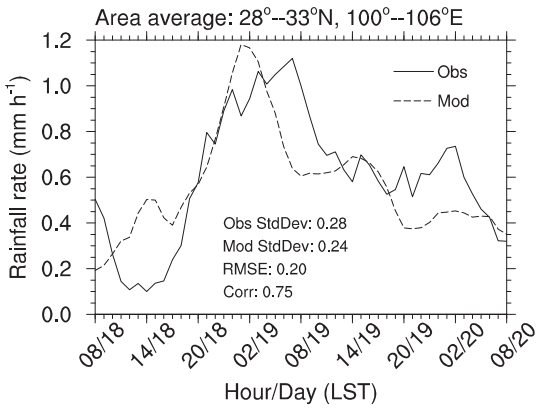

Fig. 1. Time series of area averaged (28°–33°N, 100°–106°E) observation (solid line) and model (dashed line) precipitation rate (units: mm h^{-1}) from 0800 LST 18 August to 0800 LST 20 August 2010. The standard deviation of observation precipitation rate is 0.28 mm h^{-1}, and 0.24 mm h^{-1} for model precipitation rate. The root mean square error (RMSE) and correlation coefficient between observation and model precipitation rate are 0.20 mm h^{-1} and 0.75, respectively.

The water vapor related processes are integrated into $Q_{WV} = Q_{WVL} + Q_{WVA} + Q_{WVD} + Q_{WVE}$, and the cloud-related processes are integrated into $Q_{CM} = Q_{CLL} + Q_{CLA} + Q_{CLD} + Q_{CIL} + Q_{CIA} + Q_{CID}$.

The moisture-related processes (Q_{WV}) include water vapor local change rate (Q_{WVL}), 3D moisture advection (Q_{WVA}), 3D moisture diffusion (Q_{WVD}) and surface evaporation rate (Q_{WVE}). The water vapor local change rate (Q_{WVL}) shows the contributions of vertically integrated water vapor change rate in an atmospheric column (increasing, $\frac{\partial(\rho_a Q_v)}{\partial t}$ >0 or decreasing, $\frac{\partial(\rho_a Q_v)}{\partial t}$ <0) to the surface rain rate. The 3D advection of water vapor (Q_{WVA}) mainly depicts the large-scale water vapor flux convergence/divergence which is very important to the surface rainfall (Holton and Hakim, 2013). The surface evaporation rate (Q_{WVE}) describes the moisture evaporation rate from the land or oceanic surfaces, acting as an indispensable source for the surface rainfall (Cui and Li, 2006).

The cloud-related processes (Q_{CM}) include the local change rate of liquid-phase hydrometeors (cloud water and rain water) (Q_{CLL}), 3D advection of liquid-phase hydrometeors (Q_{CLA}) which represents the flux convergence or divergence of liquid-phase hydrometeors, 3D diffusion of liquid-phase hydrometeors (Q_{CLD}), local change rate of ice-phase hydrometeors (cloud ice, snow, graupel, and hail) (Q_{CIL}), 3D advection of ice-phase hydrometeors (Q_{CIA}) which is the flux convergence or divergence of ice-phase hydrometeors, and the 3D diffusion of ice-phase hydrometeors (Q_{CID}).

The moisture-related and cloud-related processes depict the large-scale water vapor contributions and cloud-related contributions to the surface rainfall processes, respectively. The surface precipitation equation connects the water vapor budget and the cloud hydrometeor budget directly to the surface rain rate, which is very helpful to thoroughly understand the physical processes and mechanisms in surface precipitation.

Compared with the CRM-based surface rainfall equation in the 2D framework (Gao et al., 2005), the 3D WRF-based surface precipitation equation here presents similar expressions and physical meanings to the 2D equation. However, some differences do exist between this 3D equation and the equation in the 2D framework proposed by Gao et al. (2005). They include not only the dimensionality but also some sub-terms in the two equations, such as the diffusion terms, the advection terms of hydrometeors and the detailed divisions (liquid-phase and ice-phase processes) of cloud-related terms (Q_{CM}), which should be more intact and precise for the analysis of precipitation processes in the atmosphere.

3. Surface rainfall processes and roles of surface evaporation in a torrential rain event

In this section, the newly obtained 3D WRF-based surface precipitation equation is applied to the analysis of a torrential rain event in Sichuan, China from 0200 LST (Local Standard Time, UTC + 8 h) 18 August to 0800 LST 20 August 2010 to thoroughly understand the physical processes and mechanisms of the heavy rainfall. The rainfall event has been successfully simulated by Li et al. (2014) and Huang and Cui (2015) using the WRF model with similar model setups. The model was integrated for 54 hours from 0200 LST 18 August to 0800 LST 20 August 2010 using three nests with resolutions of 27, 9, and 3 km, respectively (Huang and Cui, 2015). Within the 3-km domain, only the cloud microphysical parameterization scheme, the Milbrandt 2-mom scheme (Milbrandt and Yau, 2005a,2005b), was used. The WRF model reproduced the heavy rainfall event well. For simulation verification and other details of the simulations, please refer to Li et al. (2014) and Huang and Cui (2015). In this study, each term in the 3D WRF-based surface precipitation equation was calculated by using the output from the WRF model and analyzed below.

It deserves to be specially noted that, compared with the previous somewhat idealized modeling study using the 2D CRM (Cui, 2008, 2009; Cui and Li, 2006, 2009; Gao et al., 2009; Gao and Li, 2008b, 2010; Li, 2006; Li et al., 2011; Shen et al., 2014; Wang et al., 2007, 2010), this study using the WRF model and the 3D surface precipitation equation considers not only the real topography but also spatially and temporally varying initial fields.

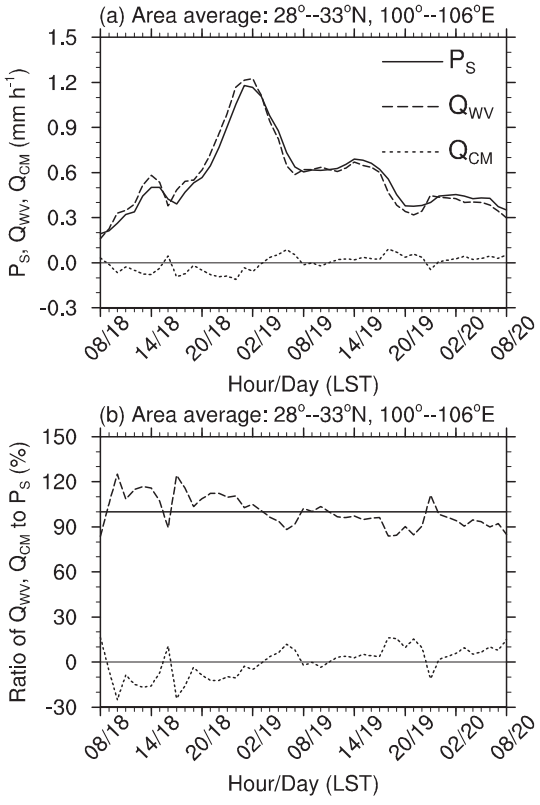

Fig. 2. (a) Time series of area averaged (28°–33°N, 100°–106°E) P_S (solid line), Q_{WV} (dashed line) and Q_{CM} (dot line) (units: mm h^{-1}) from 0800 LST 18 August to 0800 LST 20 August 2010. (b) Time series of ratio of area averaged (28°–33°N, 100°–106°E) P_S (solid line), Q_{WV} (dashed line) and Q_{CM} (dot line) to P_S (units: %) from 0800 LST 18 August to 0800 LST 20 August 2010.

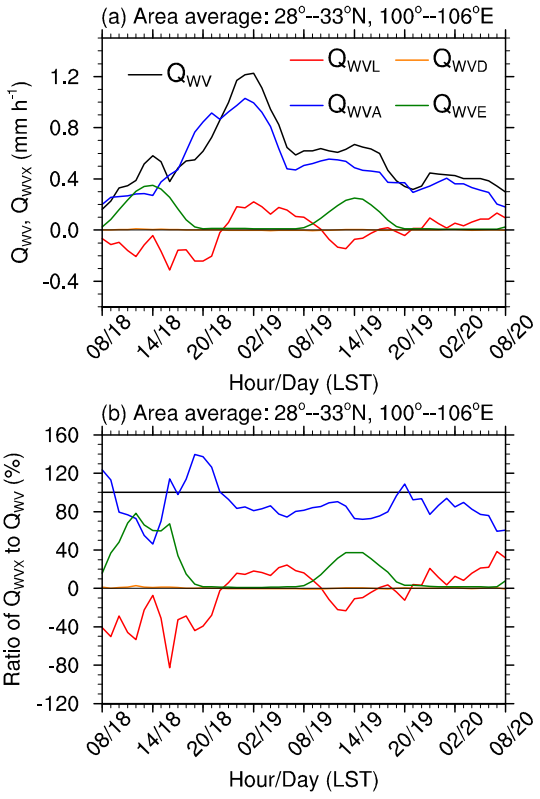

Fig. 3. (a) Time series of area averaged (28°–33°N, 100°–106°E) Q_{WV} (black line), Q_{WVL} (red line), Q_{WVA} (blue line), Q_{WVD} (orange line), and Q_{WVE} (green line) (units: mm h^{-1}) from 0800 LST 18 August to 0800 LST 20 August 2010. (b) Time series of ratio of area averaged (28°–33°N, 100°–106°E) Q_{WV} (black line), Q_{WVL} (red line), Q_{WVA} (blue line), Q_{WVD} (orange line), and Q_{WVE} (green line) to Q_{WV} (units: %) from 0800 LST 18 August to 0800 LST 20 August 2010.

3.1. surface rainfall processes

Fig. 1 shows the time series of area averaged (28°–33°N, 100°–106°E) observational and simulated rain rates from 0800 LST 18 August to 0800 LST 20 August 2010. Observations used here are hourly data produced by merging hourly precipitation observed by automatic weather stations in China and CMORPH satellite data with a 0.1° × 0.1° resolution (Pan et al., 2012; Shen et al., 2013). The time evolutions of observed and simulated area-averaged precipitation rates were generally similar (Fig. 1). The standard deviations of the observed and simulated precipitation were 0.28 mm h^{-1} and 0.24 mm h^{-1}, respectively. The root mean square error (RMSE) between them is 0.20 mm h^{-1}, which is less than the standard deviations of the observed and simulated rain rates, indicating that the precipitation from the WRF model resembles the observed precipitation. In the following parts of this paper, the WRF model output data were used to study the surface precipitation processes based on the 3D WRF-based surface precipitation equation.

Fig. 2 shows time series of simulated area averaged (28°–33°N, 100°–106°E) surface precipitation rate (P_S), the rates of moisture-related processes (Q_{WV}) and the cloud-related processes (Q_{CM}) (Fig. 2a), and ratios of them to P_S (Fig. 2b) from 0800 LST 18 August to 0800 LST 20 August 2010. In general, the moisture-related processes (Q_{WV}) are a significant portion of the surface precipitation (P_S), and the magnitude of cloud-related processes (Q_{CM}) are relatively small (Fig. 2a). However, sometimes, contributions of the cloud-related processes to the surface precipitation also play indispensable roles. For example, positive contributions of the cloud-related processes (Q_{CM}) to the surface precipitation rate (P_S) reach approximately 20% at 1800 and 2100 LST 19 August at the ending period of the heavy rainfall event. During this period, the large-scale water vapor flux convergence declined, leading to the decreasing contribution of Q_{WV} to the surface rain rates. Negative contributions can reach nearly 25% at 1000 and 1700 LST 18 August at the beginning period of the event. During this period, the large-scale water vapor flux convergence enhanced, contributing to both vigorous development of cloud systems and increase of surface rain rate (Fig. 2b).

The results shown in Fig. 2 indicate that large-scale water vapor related processes have an extremely important role in surface precipitation, but cloud-related processes cannot be neglected, especially in accurate quantitative precipitation estimates (QPE) or forecasts (QPF) of this kind of heavy rainfall events. It has also been revealed by Gao et al. (2005) in their 2D CRM modeling study of relatively long-term tropical rainfall processes based on their CRM-based surface rainfall equation. This further implies that, to thoroughly understand surface rainfall processes, both Q_{WV} and Q_{CM} should be included no matter in long-term rainfall processes over oceans or in relatively short-term heavy rainfall processes over land.

Large-scale water vapor related processes are very important in surface precipitation. However, what are the contributions of each term in the moisture-related processes? Which is the main source term for the precipitation? Fig. 3 shows the time series of simulated area averaged (28°–33°N, 100°–106°E) Q_{WV}, Q_{WVL}, Q_{WVA}, Q_{WVD}, Q_{WVE} (Fig. 3a) and ratios of them to Q_{WV} (Fig. 3b) from 0800 LST 18 August to 0800 LST 20 August 2010. Generally, the change of the water vapor flux convergence rate, Q_{WVA}, is revealed much similar to that of Q_{WV} (Fig. 3a), implying the dominant role of Q_{WVA} in the water vapor budget. This is consistent with both qualitative and quantitative analysis in many rainfall related researches in the past with or without the surface rainfall equation (Berbery and Collini, 2000; Cui and Li, 2009; Simmonds et al., 1999; Yue et al., 2009).

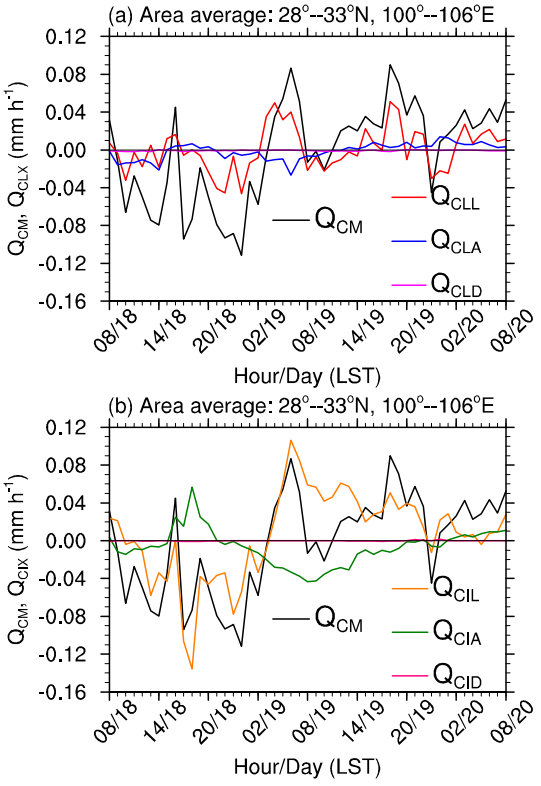

Fig. 4. Time series of area averaged (28°–33°N, 100°–106°E) Q_{CM} (black line), Q_{CLL} (red line), Q_{CLA} (blue line), Q_{CLD} (purple line), Q_{CIL} (orange line), Q_{CIA} (green line), and Q_{CID} (pink line) (units: mm h^{-1}) from 0800 LST 18 August to 0800 LST 20 August 2010.

Despite the significant role of the water vapor flux convergence (Q_{WVA}) in water vapor budget (Q_{WV}), the surface evaporation rate (Q_{WVE}) and the local change rate of water vapor (Q_{WVL}) also play indispensable roles, remarkably modulating Q_{WV}. There are two distinct peaks in Q_{WVE} during this event, at around 1400 LST 18 August (about 0.35 mm h^{-1}) and 1400 LST 19 August (about 0.25 mm h^{-1}), respectively (Fig. 3a). The change of Q_{WVE} shows some characteristics similar to diurnal variation which is very important to both climatic and synoptic researches. In rainfall-free regions, especially cloud-free regions, solar radiation warms the land surface more than the air in the daytime; thus evaporation of surface water could be enhanced (Fig. 3a). In the nighttime, the soil temperature is cooled off by infrared radiation; thus surface evaporation will reduce sharply (Fig. 3a). In the daytime, there is a lag between the increase of solar radiation and the increase of surface temperature, which should be the reason for the peak evaporation at 1400 LST. The water vapor provided by surface evaporation, especially in rainfall-free regions, moistens the atmosphere ($Q_{WVL} < 0$) and contributes indirectly to the surface rainfall through water vapor transportation from rainfall-free regions to rainfall regions (Cui and Li, 2006). In the first peak (Fig. 3), Q_{WVE} is even larger than Q_{WVA} (Fig. 3a) and the maximum ratio of Q_{WVE} to Q_{WV} could reach about 80% around 1200 LST 18 August (Fig. 3b), implying the distinct contribution of surface evaporation. The second peak of Q_{WVE} (Fig. 3a) is a little smaller than the first one. This may be resulted from the changes of radiation absorbed by the surface due to the vigorous development of cloud systems following the first peak, and also from the changes of fractions of cloud-free regions. This topic has seldom been conducted in previous studies using the CRM and related 2D rainfall equation (Cui and Li, 2006; Cui, 2008), and could be investigated thoroughly using the WRF model and the 3D WRF-based surface precipitation equation later.

As for the local change rate of water vapor (Q_{WVL}), it is basically opposite in phase with the surface evaporation rate (Q_{WVE}) (Fig. 3). During the daytime, water vapor coming from surface evaporation and large-scale convergence humidifies the atmosphere ($Q_{WVL} < 0$) as well as contributes to the surface rainfall (Fig. 3a). During the nighttime, one of the water vapor sources in the daytime, Q_{WVE}, falls to near 0 (Fig. 3a), while the continuous and even heavier surface rainfall (Fig. 2a) needs more supplements of water vapor suppliers besides the important moisture source, Q_{WVA}. Thus the atmosphere begins to get drier ($Q_{WVL} > 0$), acting as a supplementary positive contributor (moisture source) to the surface precipitation (Fig. 3a).

The surface evaporation process (Q_{WVE}) and the local drying or wetting processes of atmosphere (Q_{WVL}) may exert important regulatory but opposite roles in the surface precipitation (P_S). As mentioned above and in Cui and Li (2006), the roles of water vapor related processes, especially Q_{WVE} and Q_{WVL}, may be much different in rainfall-free regions (including cloud regions with no rain and cloud-free regions) and rainfall regions. To know more details about the roles, surface rainfall processes in both rainfall regions and rainfall-free (especially cloud-free) regions should be analyzed separately, which will be addressed in future work.

To further understand the contributions of the cloud-related processes to the surface precipitation in this event, time series of simulated area averaged (28°–33°N, 100°–106°E) Q_{CM}, Q_{CLL}, Q_{CLA}, Q_{CLD}, Q_{CIL}, Q_{CIA}, and Q_{CID} from 0800 LST 18 August to 0800 LST 20 August 2010 are illustrated in Fig. 4. The contributions of cloud-related processes are relatively smaller (Fig. 2) but more complicated compared with those of moisture-related processes (Figs. 3 and 4), implying more complex and high-frequency variations related to cloud processes. The cloud-related budget is dominated by the local change rates of liquid-phase and ice-phase cloud hydrometeors (Fig. 4). It implies that the

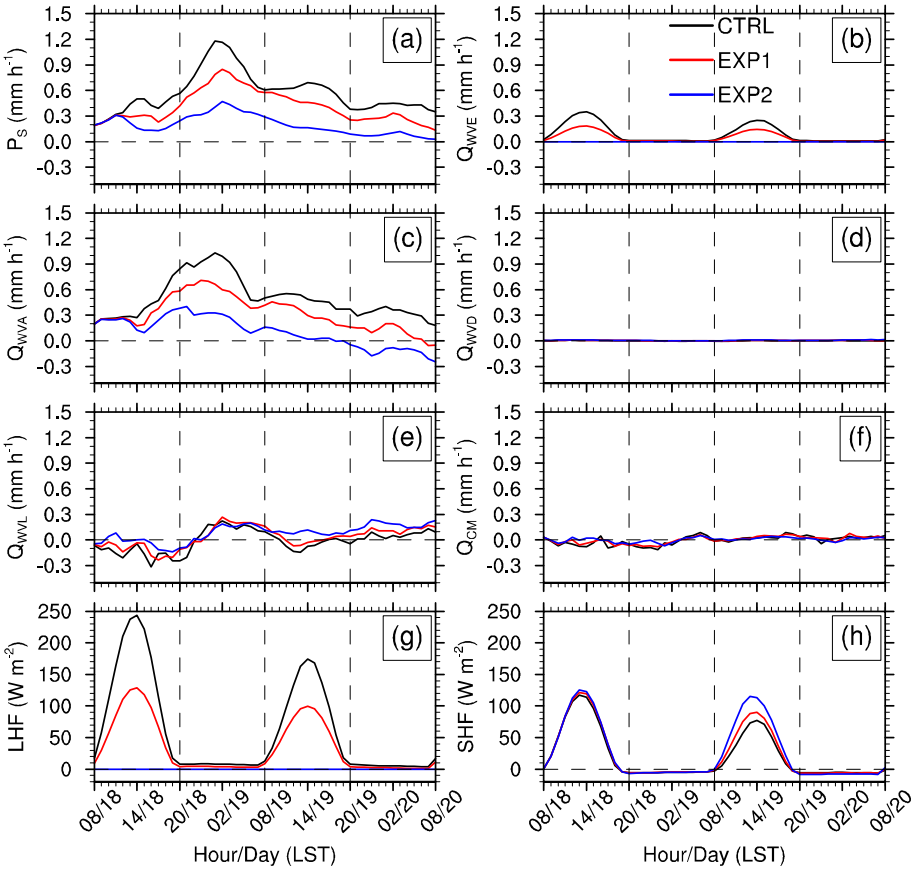

Fig. 5. Time series of area averaged (28°–33°N, 100°–106°E) P_S (a), Q_{WVE} (b), Q_{WVA} (c), Q_{WVD} (d), Q_{WVL} (e), Q_{CM} (f) (units: mm h^{-1}), LHF (surface latent heat flux, g), and SHF (surface sensible heat flux, h) (units: W m^{-2}) from 0800 LST 18 August to 0800 LST 20 August 2010 in CTRL (black line), EXP1 (red line) and EXP2 (blue line) experiments.

development of cloud systems consumes water vapor and prepares for the upcoming heavy rainfall (Fig. 2a), especially before 0200 LST 19 August. With the occurrence of the heavy rainfall, the gradual collapse of cloud systems begins to feed the surface precipitation (Figs. 2a and 4). Besides, 3D advections of hydrometeors, especially 3D advection of ice-phase hydrometeors (Q_{CIA} in Fig. 4b), also play roles in the cloud-related budget and then the surface precipitation. This was seldom addressed in the past studies using the 2D CRM-based surface rainfall equation (Cui, 2008, 2009; Cui and Li, 2006, 2009; Gao et al., 2009; Gao and Li, 2008a, 2010; Li, 2006; Wang et al., 2007).

Previous studies indicated that, cloud-mergers, especially those of convective clouds, could be an very important process to result in rainfall enhancement, and cloud split-offs may also result in collapses of rainfall systems or redistributions of heavy rainfall (Fu and Guo, 2012; Simpson et al., 1980; Tao and Simpson, 1984, 1989; Westcott, 1994). These could be investigated quantitatively using the 3D WRF-based surface precipitation equation by analyzing the variations associated with the above 3D advections of cloud hydrometeors (Q_{CLA} and Q_{CIA}). In this case, before 2000 LST 18 August, the positive Q_{CLA} and Q_{CIA} should have some relationship with cloud-mergers occurring during the development stage of cloud systems before the heavy rainfall. The negative Q_{CLA} and Q_{CIA} after that may be partially related with cloud split-offs or collapses during the heavy rainfall period (Figs. 2a and 4). Since the current study is an area-averaged analysis, the convective scale cloud mergers or split-offs may be largely smoothed out by the area mean procedure. More detailed analysis could be performed using the 3D WRF-based surface precipitation equation in higher spatiotemporal resolutions without area averaging. Partitioning methods (Sui et al., 1994; Xu, 1995) could also be applied to partition the rainfall and the moisture and cloud budgets in the 3D precipitation equation into convective and stratiform components for more in-depth analysis.

Spatially and temporally varying large-scale fields and real topography as applied in the WRF model could significantly influence the evolution of cloud and rainfall systems, including cloud-mergers and split-offs (collapses). The above kind of analyses could not be easily performed by using the 2D CRM-based surface rainfall equation (Gao et al., 2005) and the 2D CRM with spatially uniform large-scale forcing and without topography. This is due to not only the differences between dimensional features of the 2D and 3D equations but also the differences of model architectures between the CRM and the WRF model.

3.2. Sensitivity experiments on surface evaporation

In Section 3.1, it was found that surface evaporation played an important role in this rainfall event. To further understand the role of surface evaporation in the heavy rainfall, two additional sensitivity experiments were performed. All parameters of both sensitivity experiments were the same as those in the original one (hereafter CTRL experiment) except for the surface evaporation rate. The values of surface evaporation rate in the first sensitivity experiment (hereafter

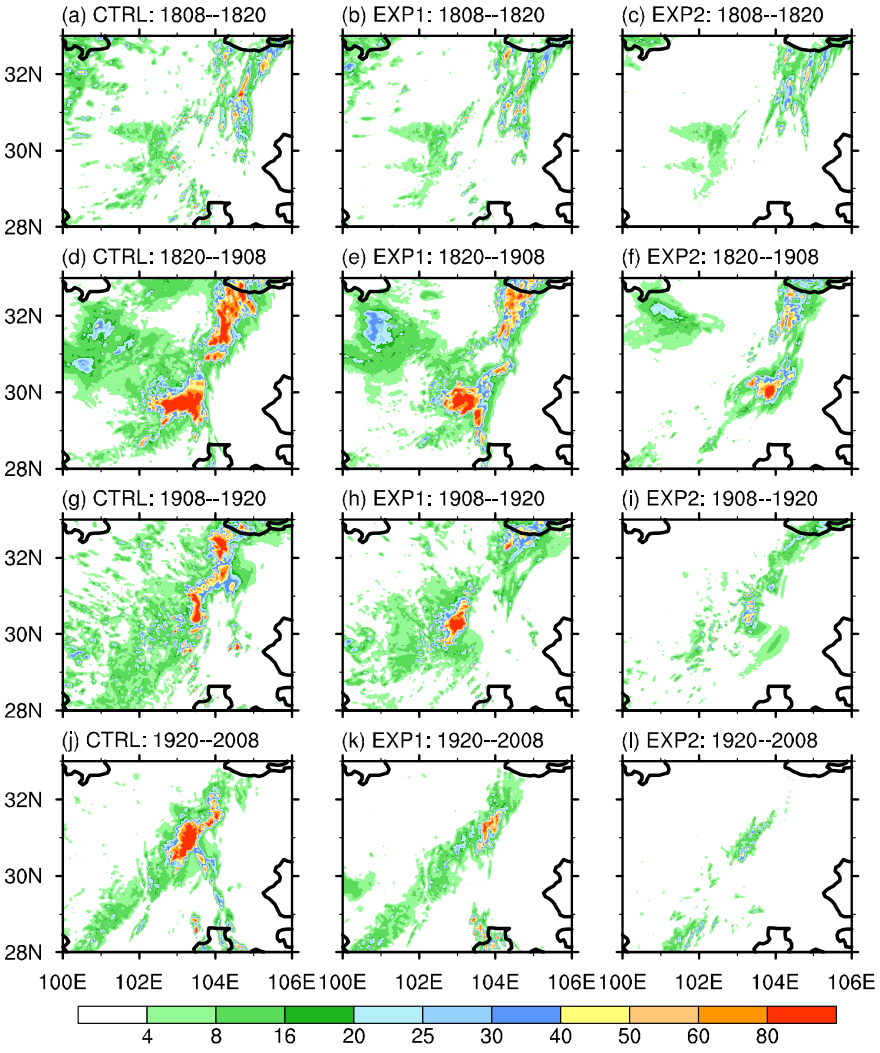

Fig. 6. 12-h accumulated precipitation (units: mm) of the CTRL experiment (left column), EXP1 experiment (center column) and EXP2 experiment (right column). a–c: 0800–2000 LST 18 August; d–f: 2000 LST 18 August to 0800 LST 19 August; g–i: 0800–2000 LST 19 August; j–l: 2000 LST 19 August to 0800 LST 20 August.

EXP1 experiment) are half of those in CTRL experiment. No surface evaporation experiment is referred to as experiment 2 (hereafter EXP2 experiment). Different responses of surface rainfall processes, cloud, dynamic and thermodynamic structures in different experiments are discussed below to further illustrate the roles of surface evaporation.

3.2.1. Responses of surface rainfall processes

Time series of area averaged (28°–33°N, 100°–106°E) P_S, Q_{WVE}, Q_{WVA}, Q_{WVD}, Q_{WVL}, Q_{CM}, surface latent heat flux (LHF), and surface sensible heat flux (SHF) from 0800 LST 18 August to 0800 LST 20 August 2010 in CTRL, EXP1 and EXP2 experiments are shown in Fig. 5. Basically, in the sensitivity experiments halving or neglecting surface evaporation rate (Q_{WVE}) (EXP1 and EXP2 in Fig. 5b), surface rain rates (P_S) are obviously weakened except for those during the beginning stage of the case. The weakening is not linear (Fig. 5a), which indicates that surface evaporation should play a nonlinear role in surface rainfall processes. The time series of P_S in both sensitivity experiments (EXP1 and EXP2) are smoothed out a lot. The main rainfall peak at around 0200 LST 19 August is markedly reduced and there are no distinct peaks of rain rates at around 1400 LST 18 August and 1400 LST 19 August as in CTRL experiment (Fig. 5a).

There are also obvious differences of Q_{WVA} among the three experiments (Fig. 5c). The area averaged water vapor flux convergences in the sensitivity experiments are markedly reduced in comparison with that in CTRL experiment. Especially in EXP2 experiment with no surface evaporation, area averaged Q_{WVA} is reduced a lot and even plays a negative role in surface precipitation after 1900 LST 19 August (blue line in Fig. 5c). This indicates that the large-scale water vapor flux divergence could coexist with surface rainfall, during which other sources of surface rainfall, including Q_{WVL} (blue line in Fig. 5e) and Q_{CM} (blue line in Fig. 5f), would contribute to the surface rain rate (blue line in Fig.5a).

Q_{WVA} and Q_{WVE} are the two main water vapor suppliers from the atmosphere outside the analyzing region and the land surface, respectively. It could be deduced that water vapor from surface evaporation could help to moisten the atmosphere (especially in rainfall-free regions where the process of surface evaporation is more vigorous (Cui and Li, 2006)), and then contribute to the rainfall through water vapor transportation from rainfall-free regions to rainfall regions (Cui and Li, 2006). This is distinctly reduced in EXP2 experiment in which one of the two suppliers, Q_{WVE}, is totally cutting off.

In Fig. 5e, with the halving and vanishing of surface evaporation, diurnal variations of water vapor local change rate (Q_{WVL}) is obviously reduced in EXP1 and EXP2 experiments, implying the concurrent characteristics (Fig. 3a) of the diurnal variation of Q_{WVL} with that of Q_{WVE}. The water vapor local change rates in EXP1 and EXP2 experiments are enhanced (or the negative rates are reduced) almost during the whole period of the event (Fig. 5e). This indicates that Q_{WVL} would compensate partially for the reduction of Q_{WVE} in EXP1 experiment and the disappearance of Q_{WVE} in EXP2 experiment, and contribute to the rainfall instead (blue line in Fig. 5e).

It is noted that the differences of Q_{WVL} among the three experiments are relatively small from 2000 LST 18 August to 0800 LST 19 August (Fig. 5e). During this period, the large-scale vertical velocities are relatively stronger (details in Section 3.2.2, Figs. 8d, e, and f) with heavier rainfall (Fig. 2a) and surface evaporation rates are almost 0 during the nighttime. This implies that the moisture both transported from outside the analyzing region and obtained from drying process of local atmosphere may contribute to the rainfall during relatively heavier rainfall period in the nighttime. Especially, from 2000 LST 19 August to 0800 LST 20 August, Q_{WVL} (blue line in Fig. 5e) would not only compensate the water vapor flux divergence (blue line in Fig. 5c) but also support the rainfall (blue line in Fig. 5a) during weaker rainfall period.

The changes of surface evaporation rates also impact the cloud-related processes (Fig. 5f) but with relatively small differences among different experiments. Meanwhile, surface sensible heat flux (SHF, Fig. 5h) presents little difference in different experiments, accompanied by distinct difference of surface latent heat flux (LHF, Fig. 5g) which is directly related with the surface evaporation rate. Small differences of SHFs appear from 0800 LST 19 August to 2000 LST 19 August, with the largest SHF in EXP2 experiment and the smallest one in CTRL experiment (Fig. 5h). The distinct collapses of cloud and rainfall systems (Fig. 5a) and the distinct reduction of the rainfall area (Fig. 6i) in EXP2 experiment may be the main cause.

The distinct differences of the surface rainfall processes among the three experiments discussed above must result in big differences of precipitation intensity and distributions (Fig. 6). The CTRL experiment with the original surface evaporation rate produces the heaviest and most widely distributed rainfall (Figs. 6a, d, g, and j). The EXP2 experiment with no surface evaporation produces the least rainfall (Figs. 6c, f, i, and l). The heavy rainfall in EXP2 experiment from 2000 LST 18 August to 0800 LST 19 August (Fig. 6f) implies the important contribution of large-scale moisture flux convergence (Fig. 5c) and the supplementary contribution of positive Q_{WVL} (Fig. 5e). Positive Q_{WVL} in EXP2 experiment continues to be active later from 0800 LST 19 August to 0800 LST 20 August (Fig. 5e), but the rain rate decreases fast (Figs. 5a, 6i and l) due to the distinct decrease of large-scale water vapor flux convergence (Fig. 5c). Moreover, the stronger the surface evaporation during the daytime is, the heavier the rainfall during the nighttime is. In short, intensity and diurnal variation of surface evaporation would affect the intensity and regional redistribution of the surface precipitation in this torrential rainfall event.

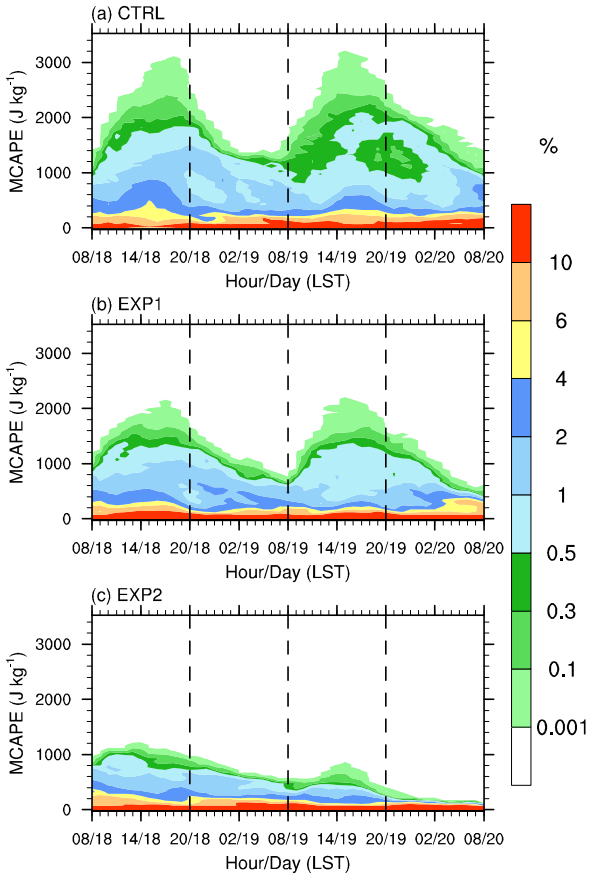

Fig. 7. Frequency of maximum convective available potential energy (MCAPE, units: J kg^{-1}) of the CTRL experiment (a), EXP1 experiment (b) and EXP2 experiment (c) from 0800 LST 18 August to 0800 LST 20 August. Contour intervals are 0.001, 0.1, 0.3, 0.5, 1, 2, 4, 6, and 10%.

3.2.2. Responses of maximum convective available potential energy, vertical velocity and radar reflectivity

As discussed above, different surface evaporation rates will make a big difference in surface rainfall processes. Surface precipitation is closely related with dynamic, thermodynamic and cloud structures. What are the responses of dynamic, thermodynamic and cloud structures to different surface evaporation rates? This is the question to be answered in detail below.

Maximum convective available potential energy (MCAPE, the convective available potential energy calculated only for the parcel with the maximum equivalent potential temperature in the column) is used below to investigate the possible impact of surface evaporation on atmospheric stability in this event. Fig. 7 shows the frequencies of the MCAPEs in CTRL, EXP1, and EXP2 experiments from 0800 LST 18 August to 0800 LST 20 August. Basically, the stronger the surface evaporation is, the broader the MCAPE distributes and the larger the MCAPE is (Fig. 7). The MCAPEs also present similar diurnal variations to a certain extent as surface evaporation, with larger MCAPEs during the daytime and smaller ones during the nighttime. In CTRL experiment, with the enhancement of surface evaporation (Fig. 5b) and surface latent heat flux (Fig. 5g) during the daytime, MCAPE increases rapidly and reaches its maximum (over 3100 J kg^{-1}) at around 1800 LST 18 August and 1500 LST 19 August, indicating that atmospheric unstable energy accumulates quickly (Fig. 7a). On the contrary, MCAPE increases slowly in EXP1 experiment, and its maximum is about 2200 J kg^{-1} (Fig. 7b). MCAPE increases the most slowly in EXP2 experiment with no surface evaporation (Fig. 7c). During the nighttime (2000 LST 18 August to 0800 LST 19 August and 2000 LST 19 August to 0800 LST 20 August), MCAPE decreases quickly, especially in CTRL experiment (Fig. 7), indicating the releases of convective available potential energy with the occurrence of surface rainfall.

The accumulation of convective available potential energy is closely related to the surface evaporation in this torrential rainfall event. It can enhance the instability of the atmosphere, which provides favorable energy conditions for the development of convection systems. It should be noted that the accumulation of instability energy is only one of the favorable conditions for surface rainfall. The maximums of MCAPEs during 0800 LST 18 August to 2000 LST 18 August and 0800 LST 19 August to 2000 LST 19 August are similar in CTRL (EXP1) experiment (Fig. 7). However, the rainfall intensities in the following periods (2000 LST 18 August to 0800 LST 19 August and 2000 LST 19 August to 0800 LST 20 August) are much different (Figs. 5a and 6) in both CTRL and EXP1 experiments. This implies that other complex dynamic or thermodynamic factors (such as large-scale convergences in Fig. 5c and vertical motions) should take distinct effects in the rainfall processes.

Yuter and Houze (1995) proposed the contoured frequency by altitude diagrams (CFADs) to examine statistical changes in vertical distributions of storm properties. The statistical method has been widely used to quantify vertical variations of numerous variables in different types of storms and examine model fields (Rauber et al., 2014; Rogers et al., 2015; Wang and Wang, 2014; Zeng et al., 2001). The CFADs of vertical velocity (Fig. 8) and radar reflectivity (Fig. 9) in the three experiments are used to investigate the responses of 3D dynamic and cloud structures to different surface evaporation rates.

Fig. 8 shows a broader distribution of vertical velocity in CTRL experiment than those in EXP1 and EXP2 experiments. In CTRL experiment, maximum ascending velocity reaches 10 m s^{-1} at around 9 km whereas

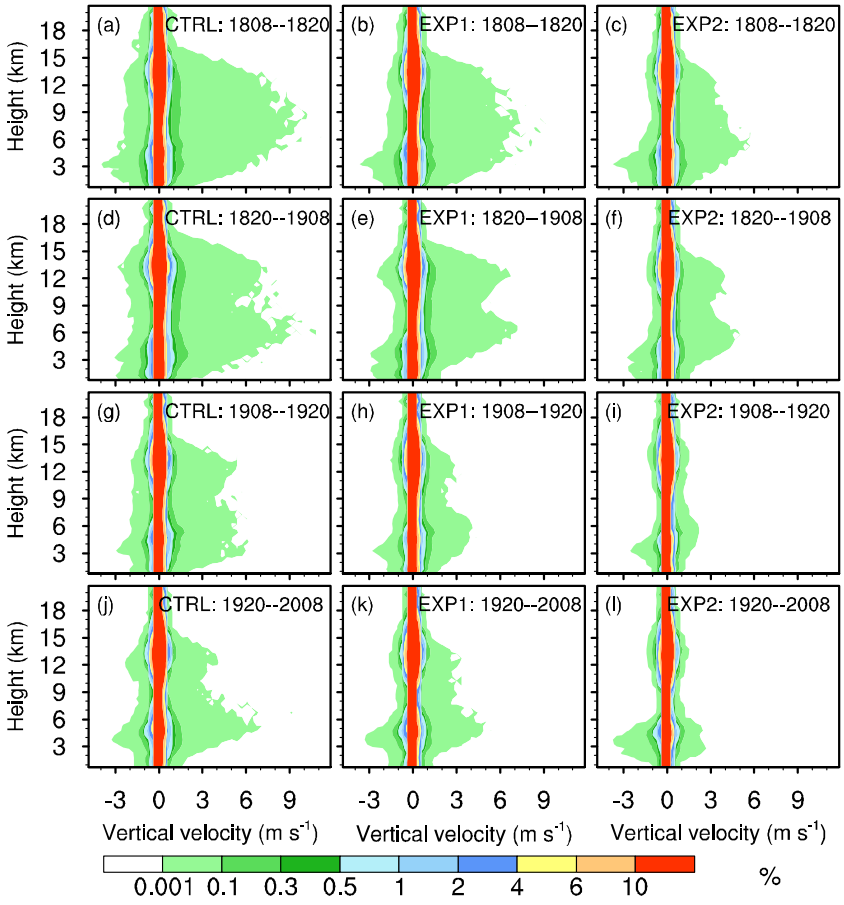

Fig. 8. Contoured frequency by altitude diagrams (CFADs) of vertical velocity (units: m s^{-1}) of the CTRL experiment (left column), EXP1 experiment (center column) and EXP2 experiment (right column). a–c: 0800–2000 LST 18 August; d–f: 2000 LST 18 August to 0800 LST 19 August; g–i: 0800–2000 LST 19 August; j–l: 2000 LST 19 August to 0800 LST 20 August. Contour intervals are 0.001, 0.1, 0.3, 0.5, 1, 2, 4, 6, and 10%.

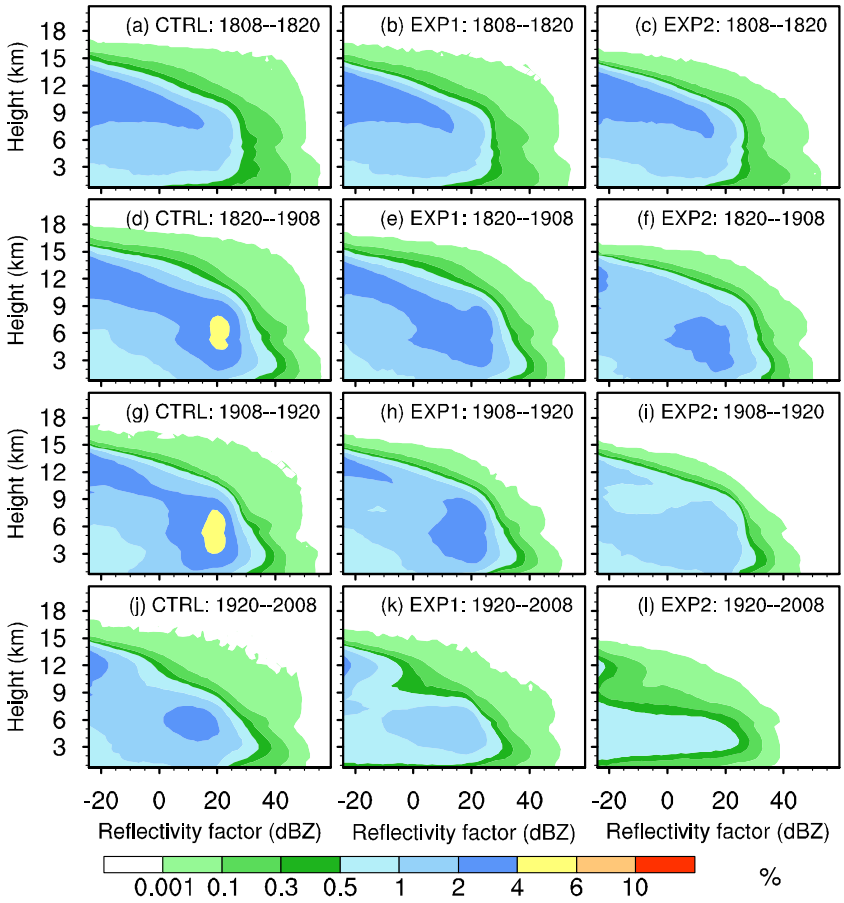

Fig. 9. Contoured frequency by altitude diagrams (CFADs) of radar reflectivity factor (units: dBZ) of the CTRL experiment (left column), EXP1 experiment (center column) and EXP2 experiment (right column). a–c: 0800–2000 LST 18 August; d–f: 2000 LST 18 August to 0800 LST 19 August; g–i: 0800–2000 LST 19 August; j–l: 2000 LST 19 August to 0800 LST 20 August. Contour intervals are 0.001, 0.1, 0.3, 0.5, 1, 2, 4, 6, and 10%.

the maximum descending velocity is about 4 m s^{-1} at around 3 km during 0800 LST 18 August to 2000 LST 18 August (Fig. 8a). In EXP2 experiment, the maximum ascending motion is obviously weaker (about 5.5 m s^{-1} at around 6 km) and the maximum descending motion is similar to those in CTRL and EXP1 experiments (Fig. 8c). Strong ascending motions in the early stages of heavy rainfall events are conducive to the development of cloud systems. Therefore, it can be seen that a broader and higher distributions of radar reflectivity in CTRL and EXP1 experiments than in EXP2 experiment during 0800 LST 18 August to 2000 LST 18 August (Figs. 9a–c). However, in this period, differences of reflectivity distributions among the three experiments are not significant, and their 12-h accumulated precipitation distributions are also similar (Figs. 6a–c). This may be because that the effects of changed surface evaporation rates have not been thoroughly showed out during the beginning period of the heavy rainfall case.

During 2000 LST 18 August to 0800 LST 19 August, late evening to early morning, precipitation intensity enhanced significantly (Figs. 6d–f). Distributions of ascending motions have two peaks at around 6 km and 12 km in all the three experiments, but the maximum ascending motions are unabated compared with those in the previous period (Figs. 8d–f). Meanwhile, more than 4% of reflectivity in CTRL experiment reaches 20 dBZ between 4 km and 8 km, and the contours 2 of CFADs in EXP1 and EXP2 experiments have also been extended to 20 dBZ (Figs. 9d–f). In this period, surface precipitation rates reached their peaks (Fig. 5a), and there were broad distributions of reflectivity throughout the troposphere in all experiments (Figs. 9d–f). This indicates that the cloud systems achieved the most exuberant development stage.

During 0800 to 2000 LST 19 August, vertical motions began to weaken significantly (Figs. 8g–i), and distributions of reflectivity also began to narrow gradually (Figs. 9g–i) in all experiments. While there was still broader distribution of reflectivity throughout the troposphere in CTRL experiment (Fig. 9g), and 12-h accumulated precipitation was larger in CTRL experiment than those in EXP1 and EXP2 experiments (Figs. 6 g–i). In this period, precipitation intensity abated in all the three experiments. In the last period from 2000 LST 19 August to 0800 LST 20 August, distributions of vertical motion in the three experiments changed little and even strengthened in the lower troposphere (Figs. 8j–l), but distribution ranges of reflectivity obviously reduced (Figs. 9j–l), while vertical motions or radar reflectivity in CTRL experiment were still stronger than those in EXP1 and EXP2 experiments.

Overall, surface evaporation exerts distinct impacts on the developments of MCAPE, vertical motions and cloud systems, as well as the budgets of both water vapor and cloud, and then affects the surface precipitation. This suggests that accurate estimation of surface evaporation is necessary for accurate simulation and forecast of surface precipitation, and surface evaporation cannot be ignored in the short-term heavy rainfall event.

4. Summary and conclusions

In this study, surface rainfall equation previously derived in a 2D CRM framework (Gao et al., 2005) was expanded into the 3D WRF framework. Compared with the 2D CRM-based surface rainfall equation, the newly obtained 3D WRF-based surface precipitation equation could

better describe the dynamic and thermodynamic characteristics of real atmosphere. The 3D surface precipitation equation was then used to examine the surface rainfall processes of a torrential rainfall event in Sichuan, China using high-resolution simulation data by the WRF model. Moreover, two additional sensitivity experiments were performed to further explore the roles of surface evaporation in the heavy rainfall event. The major results can be summarized as follows:

(1) The contributions of moisture-related processes to the surface precipitation (Q_{WV}) dominate the torrential rainfall event, but the contributions of cloud-related processes (Q_{CM}) also play indispensable roles whose maximum net contributions could exceed 20% in this case. To thoroughly understand surface rainfall processes, both Q_{WV} and Q_{CM} should be included no matter in long-term rainfall processes over oceans (Cui, 2008; Cui and Li, 2006; Gao and Li, 2008a, 2010; Li, 2006) or in relatively short-term heavy rainfall processes over land.
(2) Q_{WVA} plays a dominant role in the water vapor budget, while Q_{WVL} and Q_{WVE} also play important roles and cannot be ignored in this event. Sometimes, Q_{WVE} could be even larger than Q_{WVA}, with maximum ratio of Q_{WVE} to Q_{WV} reaching about 80%, and the maximum positive/negative ratios of Q_{WVL} to Q_{WV} could reach 40% and 80%, respectively. The change of Q_{WVE} with time shows some diurnal variation characteristics. The contributions of cloud-related processes are relatively smaller but more complex compared with those of moisture-related processes in this event. The cloud-related processes are dominated by local change rate of liquid-phase and ice-phase cloud hydrometeors. Besides, 3D advection of cloud hydrometeors, especially that of ice-phase cloud hydrometeors, also plays a role in the surface precipitation.
(3) Sensitivity experiments show that surface evaporation has a considerable effect on the short-term heavy rainfall event. It affects both the water vapor budget and the cloud hydrometeor budget, and then the intensity and regional redistribution of the surface precipitation.
(4) Surface evaporation can affect the accumulation of convective available potential energy in this torrential rainfall event. It can enhance the instability of the atmosphere, which provides favorable energy conditions for the development of convection systems. Besides, surface evaporation also has an important influence on the development of vertical motions and cloud systems, and then affects surface precipitation. This suggests that accurate estimation of surface evaporation is much necessary for accurate simulation and forecast of surface precipitation.

Acknowledgments

Yongjie Huang and Xiaopeng Cui were supported by the Key Research Program of the Chinese Academy of Sciences (Grant No. KZZD-EW-05-01) and the National Basic Research Program of China (973 Program) (Grant Nos. 2015CB452804 and 2014CB441402). Xiaopeng Cui and Xiaofan Li were supported by National Natural Science Foundation of China under Grant Nos. 41175056 and 41475039 and National Key Basic Research Program of China under Grant No. 2015CB953601. The work was carried out at National Supercomputer Center in Tianjin, and the calculations were performed on TianHe-1(A). The authors are grateful to NCAR's Data Support Section providing NCEP FNL data (http://rda.ucar.edu/datasets/ds083.2/) and China Meteorological Data Sharing Service System for providing hourly precipitation observed by automatic weather stations in China merging with CMORPH satellite data (http://data.cma.gov.cn). The authors also thank two anonymous reviewers for their helpful comments on the manuscript.

References

Berbery, E.H., Collini, E.A., 2000. Springtime precipitation and water vapor flux over southeastern South America. Mon. Weather Rev. 128, 1328–1346.
Cui, X.P., 2008. A cloud-resolving modeling study of diurnal variations of tropical convective and stratiform rainfall. J. Geophys. Res.-Atmos. 113, D2–D4. http://dx.doi.org/10.1029/2007JD008990.
Cui, X.P., 2009. Quantitative diagnostic analysis of surface rainfall processes by surface rainfall equation. Chin. J. Atmos. Sci. 33, 375–387 (in Chinese).
Cui, X.P., Li, X.F., 2006. Role of surface evaporation in surface rainfall processes. J. Geophys. Res.-Atmos. 111, D17. http://dx.doi.org/10.1029/2005jd006876.
Cui, X.P., Li, X.F., 2009. Diurnal responses of tropical convective and stratiform rainfall to diurnally varying sea surface temperature. Meteorog. Atmos. Phys. 104, 53–61.
Cui, X.P., Li, X.F., 2011. A cloud-resolving modeling study of short-term surface rainfall processes. Meteorog. Atmos. Phys. 111, 1–11.
Fu, D.H., Guo, X.L., 2012. A cloud-resolving simulation study on the merging processes and effects of topography and environmental winds. J. Atmos. Sci. 69, 1232–1249.
Gao, S.T., Li, X.F., 2008a. Cloud-resolving modeling of convective processes. Springer, Dordrecht (206 pp. http://dx.doi.org/10.1007/978-1-4020-8276-4).
Gao, S.T., Li, X.F., 2008b. Precipitation efficiency, cloud-resolving modeling of convective processes. Springer, Dordrecht, pp. 137–146 (http://dx.doi.org/10.1007/978-1-4020-8276-4_9).
Gao, S.T., Li, X.F., 2010. Precipitation equations and their applications to the analysis of diurnal variation of tropical oceanic rainfall. J. Geophys. Res.-Atmos. 115. http://dx.doi.org/10.1029/2009jd012452.
Gao, S.T., Cui, X.P., Zhou, Y.S., Li, X.F., 2005. Surface rainfall processes as simulated in a cloud-resolving model. J. Geophys. Res.-Atmos. 110, D10. http://dx.doi.org/10.1029/2004jd005467.
Gao, S.T., Cui, X.P., Li, X.F., 2009. A modeling study of diurnal rainfall variations during the 21-day period of TOGA COARE. Adv. Atmos. Sci. 26, 895–905.
Grabowski, W.W., Wu, X.Q., Moncrieff, M.W., Hall, W.D., 1998. Cloud-resolving modeling of cloud systems during phase III of GATE. Part II: Effects of resolution and the third spatial dimension. J. Atmos. Sci. 55, 3264–3282.
Holton, J.R., Hakim, G.J., 2013. An introduction to dynamic meteorology. fifth ed. Academic press.
Huang, Y., Cui, X., 2015. Dominant cloud microphysical processes of a torrential rainfall event in Sichuan. Chin. Adv. Atmos. Sci. 32, 389–400.
Krueger, S.K., 1988. Numerical-simulation of tropical cumulus clouds and their interaction with the subcloud layer. J. Atmos. Sci. 45, 2221–2250.
Li, X., 2006. Cloud microphysical and precipitation responses to a large-scale forcing in the tropical deep convective regime. Meteorog. Atmos. Phys. 94, 87–102.
Li, X.F., Shen, X.Y., Liu, J., 2011. A partitioning analysis of tropical rainfall based on cloud budget. Atmos. Res. 102, 444–451.
Li, Q., Cui, X.P., Cao, J., 2014. The observational analysis and numerical simulation of a heavy rain event in Sichuan Province. Chin. J. Atmos. Sci. 38, 1095–1108. http://dx.doi.org/10.3878/j.issn.1006-9895.1401.13255 (in Chinese).
Milbrandt, J.A., Yau, M.K., 2005a. A multimoment bulk microphysics parameterization. Part I: Analysis of the role of the spectral shape parameter. J. Atmos. Sci. 62, 3051–3064.
Milbrandt, J.A., Yau, M.K., 2005b. A multimoment bulk microphysics parameterization. Part II: A proposed three-moment closure and scheme description. J. Atmos. Sci. 62, 3065–3081.
Paegle, J., Mo, K.C., Nogués-Paegle, J., 1996. Dependence of simulated precipitation on surface evaporation during the 1993 United States summer floods. Mon. Weather Rev. 124, 345–361.
Pan, Y., Shen, Y., Yu, J.J., Zhao, P., 2012. Analysis of the combined gauge-satellite hourly precipitation over China based on the OI technique. Acta. Meteor. Sin. 70, 1381–1389. http://dx.doi.org/10.11676/qxxb2015.010 (in Chinese).
Rauber, R.M., et al., 2014. Finescale radar and airmass structure of the comma head of a continental winter cyclone: The role of three airstreams. Mon. Weather Rev. 142, 4207–4229.
Rogers, R.F., Reasor, P.D., Zhang, J.A., 2015. Multiscale structure and evolution of hurricane earl (2010) during rapid intensification. Mon. Weather Rev. 143, 536–562.
Shen, X.Y., Zhang, N., Li, X.F., 2011a. Effects of large-scale forcing and ice clouds on pre-summer heavy rainfall over southern China in June 2008: A partitioning analysis based on surface rainfall budget. Atmos. Res. 101, 155–163.
Shen, X.Y., Wang, Y., Li, X.F., 2011b. Effects of vertical wind shear and cloud radiative processes on responses of rainfall to the large-scale forcing during pre-summer heavy rainfall over southern China. Q. J. R. Meteorol. Soc. 137, 236–249.
Shen, X.Y., Wang, Y., Li, X.F., 2011c. Radiative effects of water clouds on rainfall responses to the large-scale forcing during pre-summer heavy rainfall over Southern China. Atmos. Res. 99, 120–128.
Shen, Y., Pan, Y., Yu, J.J., Zhao, P., Zhou, Z.J., 2013. Quality assessment of hourly merged precipitation product over China. Trans. Atmos. Sci. 36, 37–46 (in Chinese).
Shen, X.Y., Huang, W., Qing, T., Huang, W.Y., Li, X.F., 2014. A modified scheme that parameterizes depositional growth of ice crystal: A modeling study of pre-summer torrential rainfall case over Southern China. Atmos. Res. 138, 293–300.
Simmonds, I., Bi, D.H., Hope, P., 1999. Atmospheric water vapor flux and its association with rainfall over China in summer. J. Clim. 12, 1353–1367.
Simpson, J., Westcott, N.E., Clerman, R.J., Pielke, R.A., 1980. On cumulus mergers. Arch. Meteor. Geophys. A. 29, 1–40.
Skamarock, W., Klemp, J., Dudhia, J., Gill, D., Barker, D., 2008. A description of the Advanced Research WRF version 3. NCAR Tech., Note NCAR/TN-475 + STR (p. 113pp).
Sui, C.H., Lau, K.M., Tao, W.K., Simpson, J., 1994. The tropical water and energy cycles in a cumulus ensemble model.1. Equilibrium climate. J. Atmos. Sci. 51, 711–728.

Tao, W.K., Simpson, J., 1984. Cloud interactions and merging — numerical simulations. J. Atmos. Sci. 41, 2901–2917.
Tao, W.K., Simpson, J., 1989. Modeling study of a tropical squall-type convective line. J. Atmos. Sci. 46, 177–202.
Tao, W.K., Simpson, J., Soong, S.T., 1987. Statistical properties of a cloud ensemble — a numerical study. J. Atmos. Sci. 44, 3175–3187.
Tompkins, A.M., 2000. The impact of dimensionality on long-term cloud-resolving model simulations. Mon. Weather Rev. 128, 1521–1535.
Wang, H., Wang, Y.Q., 2014. A numerical study of typhoon Megi (2010). Part I: Rapid Intensification. Mon. Weather Rev. 142, 29–48.
Wang, J.J., Li, X.F., Carey, L.D., 2007. Evolution, structure, cloud microphysical, and surface rainfall processes of monsoon convection during the South China Sea monsoon experiment. J. Atmos. Sci. 64, 360–380.
Wang, D.H., Li, X.F., Tao, W.K., 2010. Cloud radiative effects on responses of rainfall to large-scale forcing during a landfall of severe tropical storm Bilis (2006). Atmos. Res. 98, 512–525.
Westcott, N.E., 1994. Merging of convective clouds — cloud initiation, bridging, and subsequent growth. Mon. Weather Rev. 122, 780–790.
Xu, K.M., 1995. Partitioning mass, heat, and moisture budgets of explicitly simulated cumulus ensembles into convective and stratiform components. J. Atmos. Sci. 52, 551–573.
Xu, K.M., Randall, D.A., 1996. Explicit simulation of cumulus ensembles with the GATE phase III data: Comparison with observations. J. Atmos. Sci. 53, 3710–3736.
Xu, K.M., Arakawa, A., Krueger, S.K., 1992. The macroscopic behavior of cumulus ensembles simulated by a cumulus ensemble model. J. Atmos. Sci. 49, 2402–2420.
Xu, K.M., et al., 2002. An intercomparison of cloud-resolving models with the atmospheric radiation measurement summer 1997 intensive observation period data. Q. J. Roy. Meteor. Soc. 128, 593–624.
Xu, K.M., et al., 2005. Modeling springtime shallow frontal clouds with cloud-resolving and single-column models. J. Geophys. Res.-Atmos. 110, D15. http://dx.doi.org/10.1029/2004jd005153.
Yue, C.J., Shou, S.W., Li, X.F., 2009. Water vapor, cloud, and surface rainfall budgets associated with the landfall of typhoon Krosa (2007): A two-dimensional cloud-resolving modeling study. Adv. Atmos. Sci. 26, 1198–1208.
Yuter, S.E., Houze, R.A., 1995. 3-Dimensional kinematic and microphysical evolution of Florida cumulonimbus. 2. Frequency-distributions of vertical velocity, reflectivity, and differential reflectivity. Mon. Weather Rev. 123, 1941–1963.
Zeng, Z.X., Yuter, S.E., Houze, R.A., Kingsmill, D.E., 2001. Microphysics of the rapid development of heavy convective precipitation. Mon. Weather Rev. 129, 1882–1904.